Philip Ruff, Christian Dietz, Robert W. Stark and Christian Hess*

Monitoring the Process of Nanocavity Formation on a Monomolecular Level

https://doi.org/10.1515/zpch-2017-1055
Received October 17, 2017; accepted March 19, 2018

Abstract: Controlling the synthesis of nanostructured surfaces is essential to tailor the properties of functional materials such as catalysts. We report on the synthesis of nanocavities of 1–2 nm dimension on planar Si-wafers by sacrificial nanotemplating and atomic layer deposition (ALD). It is shown that the process of nanocavity formation can be directly monitored on a monomolecular level through imaging with an atomic force microscope (AFM). In particular, by employing the AFM peak force tapping mode the simultaneous mapping of surface topography and tip-surface adhesion forces is accessible, which is useful for the assignment of topographical features and determining the orientation of the template molecules on the wafer surface. Detailed analysis based on the three-dimensional AFM topography allows for a quantification of the template and nanocavity surface coverage. The results are of importance for a detailed understanding of the processes underlying template-based nanocavity formation on oxide surfaces.

Keywords: atomic force microscopy; atomic layer deposition; controlled synthesis; nanocavity; nanostructured surfaces; oxide surfaces; surface characterization.

1 Introduction

Tailor-made nanostructured materials are of great relevance for applications such as heterogeneous catalysis, electrics, photovoltaics or sensors [1–3]. Regarding heterogeneous catalysis, for example, nanostructured surfaces are essential to improve the turnover rate, selectivity, and lifetime of a catalyst [1, 4–6]. To

***Corresponding author: Christian Hess,** Eduard-Zintl-Institut für Anorganische und Physikalische Chemie, Technische Universität Darmstadt, Alarich-Weiss-Str. 8, 64287 Darmstadt, Germany, e-mail: hess@pc.chemie.tu-darmstadt.de
Philip Ruff: Eduard-Zintl-Institut für Anorganische und Physikalische Chemie, Technische Universität Darmstadt, Alarich-Weiss-Str. 8, 64287 Darmstadt, Germany
Christian Dietz and Robert W. Stark: Institute of Materials Science, Technische Universität Darmstadt, Alarich-Weiss-Str. 16, 64287 Darmstadt, Germany

this end chemical or physical techniques are necessary, which allow for high-precision structuring, ideally on an atomic scale. In this context, chemical vapor deposition (CVD) and atomic layer deposition (ALD) have proven to be most useful for the thin film and nanoparticle deposition of metals and metal oxides on nearly arbitrary substrate surfaces [2, 3, 7–11]. Regarding gas-phase deposition techniques, ALD is superior to CVD when it comes to controlling film growth on an Ångstrom to nanometer scale with atomic precision. The uniqueness of the ALD process arises from the sequential application of typically two precursors in an ABAB-type-like sequence, which due to the self-limiting layer growth in each half cycle A and B, provides perfect control over the thickness of the deposited layer [7]. Besides, applying surface preparation methods such as hydrogen-passivation, lithography or templating prior to ALD allows for the creation of surface patterns with domains that are inert towards the ALD precursors. Since ALD growth is strongly inhibited in these regions, film deposition occurs selectively on the non-modified area. This technique is known as area selective ALD [3, 8, 12–15]. However, these patterning techniques are often limited to planar substrates and structures obtained are usually in the range of some 10–100 nm [3, 12–15]. Alternatively, single molecule templating approaches towards area selective ALD allow for the modification of powders and porous materials, which are of great interest for applications in catalysis owing to their large specific surface area [8, 12]. Furthermore, single molecule templating approaches offer the possibility to create cavity-like structures with a geometry that directly correspond to the shape of the template molecule. These structures are much smaller than those obtained by other methods [8, 12]. In our previous work we demonstrated the successful surface templating of mesoporous silica SBA-15 anchoring p-*tert*-butyl-calix[4]arene onto a TiO_2 surface, which was fabricated by using ALD [8]. Applying area selective ALD of Al_2O_3 upon this bottom-up approach allows the synthesis of nanocavities as illustrated in Figure 1. Calixarene can be removed subsequently by combustion at low temperature by using ozone as a strong oxidant [8].

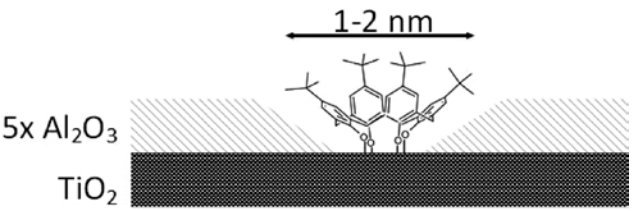

Fig. 1: Schematic illustration of the template based bottom-up synthesis of nanocavities using p-*tert*-butyl-calix[4]arene as a sacrificial template.

It is a challenge to establish direct microscopic evidence for the presence of nanocavities owing to their small size of approximately 1–2 nm. Thus, previous characterization of the synthesis pathway was done indirectly by employing spectroscopic techniques such as FTIR and UV-Vis for detecting the presence/absence of calixarene as well as the deposition of the Al_2O_3 wall material [8]. In this work we used an atomic force microscope (AFM) to directly monitor the formation of nanocavities on a molecular level. For this purpose planar Si(100) wafers were decorated with nanocavities according to Figure 1. Using the AFM peak force tapping mode further allowed us to differentiate between calixarene and the bare surface based on the variation of the tip-surface interaction between hydrophilic and hydrophobic domains [16, 17].

2 Experimental

2.1 Atomic force microscope (AFM) imaging

Atomic force microscopy surface studies were carried out using a Dimension Icon microscope (Bruker AXS, Santa Barbara, CA, USA). Topography and adhesion maps were acquired in the peak force tapping mode using "ScanAsyst Fluid" cantilevers from Bruker AXS. The inverse optical lever sensitivity was $\sigma = 40 \pm 6$ nm/V as measured on a stiff sapphire surface. The force constant of the cantilever was $k = 1.6 \pm 0.2$ N/m as determined by using the thermal noise method [18]. We applied maximum loads of $F_{peak} = 300$ pN to the samples and scanned with a rate of 1 line per second. Topography images were first order flattened to remove sample tilt and to correct for thermal drifts during the measurement. PeakForce tapping is based on force-versus-distance measurements collected with an acquisition rate of 0.5–2 kHz (500–2000 curves/s) creating two-dimensional arrays containing one force-versus-distance curve at each pixel similar to the pulsed force or jumping mode [19–21]. The maximum (not averaged) force applied to the surface during one oscillation cycle is controlled by the topographical feedback mechanism. This mode can provide maps of quantitative mechanical properties such as elastic modulus, sample deformation or adhesion simultaneously.

2.2 X-ray photoelectron spectroscopy (XPS)

X-ray photoelectron spectra were acquired on a SSX 100 ESCA spectrometer (Surface Science Laboratories Inc.) employing a monochromatic Al-K_α X-ray

source (1486.6 eV). Spectra were recorded in the constant analyzer energy (CAE) mode at a 36° detection angle. The X-ray source was operating at 9 kV and 10 mA at $<10^{-8}$ Torr base pressure of the analysis chamber. The spot size was approximately 1×0.25 mm. Detailed spectra (30 measurements) were recorded with 0.1 eV resolution.

2.3 Wafer pretreatment

Si(100)-wafers (Active Business Company GmbH) with a native polished SiO_2 layer of approximately 100 nm thickness were cleansed of impurities prior to surface modification. To this end, the wafers were sonicated consecutively for 5 min in chloroform, acetone, ethanol, and deionized water. For complete surface hydroxylation the wafers were boiled in deionized water for 1 h and then dried overnight in an oven at 85 °C [22].

2.4 Thermal ALD: TiO_2 coating

Self-limiting TiO_2 growth from the gas phase was achieved by employing the binary reaction of $TiCl_4$ (Sigma-Aldrich, 99.9%) and H_2O in an ALD process carried out in a self-made stainless steel reactor operating at 1.3 Torr [10]. The reactor walls were heated to 120 °C resulting in a substrate temperature of approximately 115 °C. One ALD cycle consisted of 10 s of precursor exposures of $TiCl_4$ and H_2O, separated by 30-s-long purging intervals with N_2 (99.999%). Both precursors were fed into the reaction chamber by evaporation with a valve opening time of 0.1 s. To increase the vapor pressure of $TiCl_4$ the precursor bottle was pre-heated to 40 °C. All wafers used in this study were coated by application of 80 cycles of TiO_2 (80x TiO_2) corresponding to approximately 2 nm as determined by ellipsometry.

2.5 Surface templating using p-*tert*-butyl-calix[4]arene

To create a hydrophobic nanopattern consisting of isolated covalently bound template molecules a Si(100) wafer + 80x TiO_2 was added to a mixture of 50 mg p-*tert*-butyl-calix[4]arene (Sigma-Aldrich, 95%) and 50 mL dry toluene (Sigma-Aldrich, 99.8%). The mixture was then boiled under reflux at 130 °C for 2 h. Subsequently, the wafer was washed with copious hot toluene and then sonicated in toluene for 30 min to remove non-bound excess calixarene. Finally, wafers were dried overnight in an oven at 85 °C [8, 12].

2.6 Thermal ALD: Al_2O_3 coating

The area selective gas phase deposition of Al_2O_3 serving as wall material for the nanocavities was carried out in a similar ALD process as for the deposition of TiO_2. Exposures of trimethylaluminum (TMA, Sigma-Aldrich, 97%) and H_2O were combined in a binary reaction using the same process parameters as described above for thermal ALD of TiO_2.

To produce nanocavities of an adequate height five ALD cycles were applied to prevent overcoating of the calixarene template molecules, resulting in a Al_2O_3 layer thickness of approximately 0.75 nm (growth rate = 1.5 Å/cycle) [8].

2.7 O_3 treatment

Treatment with O_3 was employed to obtain nanocavities by controlled removal of the calixarene template. To this end, the modified Si-wafer was placed in a glass vessel and heated to 130 °C using an oil bath. The vessel was then purged with 200 mL/min ozoniferous air produced by an ozone generator (Heyl Neomeris, LAB 2B). A flow of 3.5 mg O_3/L air (1.5 g O_3/h) was produced by feeding the generator with an air flow of 4 L/min ($p \approx 0.2$ bar). All wafers were treated for 12 h. Subsequently, the wafers were sonicated in toluene for 30 min to get rid of remaining calixarene fragments and other contaminations. The wafers were then dried overnight in an oven at 85 °C.

3 Results and discussion

For the investigation of the nanocavity synthesis Si-wafers were used, which were ALD coated with TiO_2 (see Figure 1). The presence of TiO_2 was confirmed by XPS. Detailed XP spectra of the Ti 2p region obtained after TiO_2 ALD (80 cycles) show the presence of Ti^{4+} (see Figure S1a). Simultaneously, no emission from the Si 2p core level was observed (see Figure S1b). This behavior strongly indicates that TiO_2 forms a conformal uniform layer, which is thick enough to completely suppress signals from the underlying SiO_2.

Figure 2 depicts different representations of the surface topography of a calixarene-loaded wafer (80x TiO_2). The scheme in Figure 2a outlines the expected surface texture that consists of randomly distributed and covalently bound calixarene molecules. The two-dimensional view in Figure 2b exhibits a distinct surface structure as indicated by various bright and dark spots representing heights (template molecules) and depths, respectively. Thus, bright regions represent single

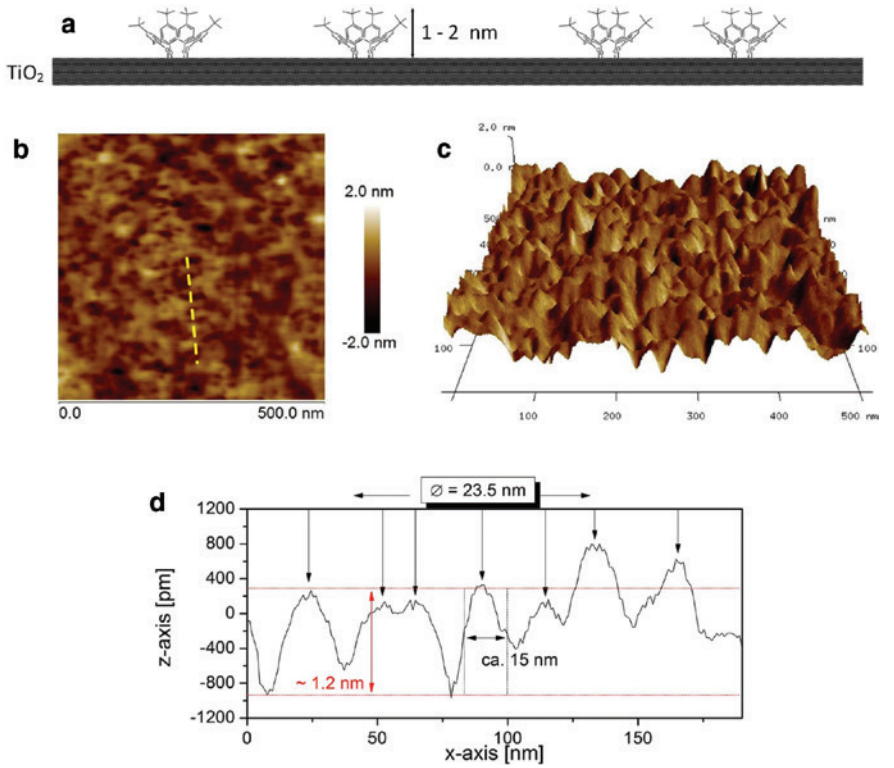

Fig. 2: Representations of the surface topography of a Si(100) wafer ALD coated with 80x TiO_2 and decorated with calixarene template molecules: (a) schematic illustration of the calixarene loaded surface, (b) 2D AFM topography, (c) 3D AFM topography, (d) cross-sectional view of the surface along the yellow trace.

isolated and agglomerated calixarene molecules on the wafer surface, while dark regions are due to unloaded areas exhibiting bare TiO_2. As compared to the reference wafer (see Figure 5), the surface provides a three-dimensional structure with a mean roughness (root mean square, RMS) of 0.39 ± 0.19 nm. Figure 2c is a three-dimensional representation of Figure 2b clearly indicating a change in the topography as compared to the originally smooth wafer surface. The cross-sectional view in Figure 2d shows distinct features with an approximate height of 1.2 nm each in accordance to the size of the calixarene molecule. Besides, the apparent width of the features results from a geometric convolution of the tip shape with the particles. Since single calixarene molecules have a size of 1–2 nm and the tip size can be estimated as 10 nm, the observed width of the features (~15 nm) fits very well to the overall picture shown in Figure 2a. Therefore, we assume that the calixarene molecules were isolated and covalently attached to

the surface rather than forming larger agglomerates consisting of several molecules, which is crucial for the formation of distinct uniform nanocavities. The mean distance between the molecules was determined as 23.5 nm by averaging the distance between maxima, which is consistent with the mean distance between nanocavities of 26.8 nm obtained from averaging the distance between minima (see Figure 3d).

Uniform nanocavities as shown in Figure 3a can be obtained upon depositing Al_2O_3 wall material in an area selective ALD approach and subsequent ozone treatment to remove calixarene. To confirm the chemical changes accompanying Al_2O_3 ALD (five cycles) and ozone treatment, XPS analyses were performed (see Figure S1). The presence of Al^{3+} subsequent to Al_2O_3 ALD is evidenced by the Al 2p photoemission (see Figure S1d), which remains unchanged upon O_3 treatment

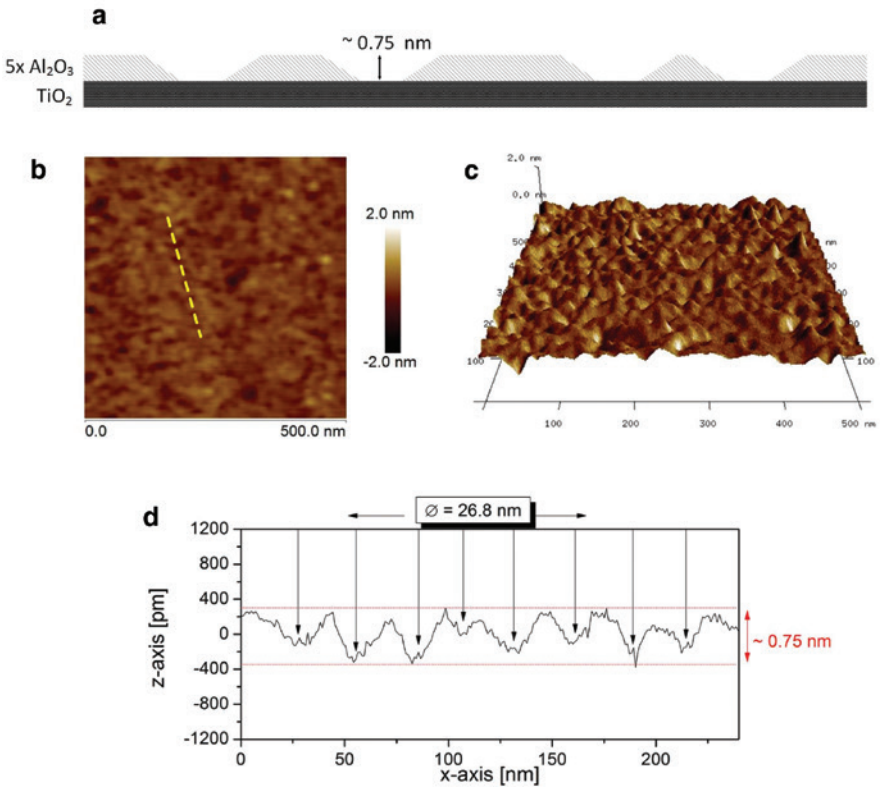

Fig. 3: Representations of the surface topography of a Si(100) wafer decorated with nanocavities: (a) schematic illustration of the surface structured with nanocavities, (b) 2D AFM topography, (c) 3D AFM topography, (d) cross-sectional view of the surface along the yellow trace.

(see Figure S1f). Besides, XP spectra also demonstrate the persistence of the TiO_2 layer (see Figure S1c and e).

The application of five Al_2O_3 ALD cycles results in a film thickness of 0.75 nm as shown previously [8]. The nanocavities synthesized here also have an expected overall depth of 0.75 nm corresponding to the Al_2O_3 layer thickness. Figure 3b provides a two-dimensional view of the modified wafer surface with a pattern of bright and dark spots representing heights and depths, respectively. As compared to the two-dimensional view of the calixarene-loaded wafer surface in Figure 2b the nanocavity-containing two-dimensional image is predominantly darker, indicating a reduced height of the features on the substrate surface. This is visualized in Figure 3c with a three-dimensional view of the surface. For comparability Figures 2c and 3c use the same scaling. It is conspicuous, that the features in Figure 2c are approximately twice as high as the features in Figure 3c. With respect to the overall picture of the bottom-up synthesis of nanocavities as presented in Figure 1 the different heights are due to their different origin. While the features in the template-loaded topography originate from calixarene molecules, the features in the nanocavity-containing topography should originate from the Al_2O_3 walls. A better awareness for this hypothesis arises from the detailed analysis and comparison of the cross-sections (see Figures 2d and 3d). The overall height of the features of the calixarene-loaded surface is approximately 1.2 nm, in agreement with the size of the calixarene molecule. On the other hand, the height of the features of the nanocavity-containing surface is approximately 0.75 nm, in agreement with the thickness of the Al_2O_3 layer. As a consequence of the reduced height of the observed features, the mean roughness has considerably decreased from 0.39 ± 0.19 nm for the calixarene-loaded wafer surface to 0.20 ± 0.14 nm for the wafer surface containing nanocavities. Furthermore, the mean distance between the cavities is 26.8 nm consistent with the mean distance between the calixarene molecules of 23.5 nm (see Figure 2d). Please note that the AFM images may display a distorted representation of the size of the cavities since the AFM tip is approximately one order of magnitude larger than the nanocavities shaped by the size of the calixarene molecules (i.e. ~1 nm vs. ~10 nm).

Recently, we demonstrated the successful formation of covalent Ti–O–C bonds resulting from the condensation of Ti–OH surface groups and C–OH calixarene groups by use of IR and UV-Vis spectroscopy [8]. The presence of Ti–O–C bonds implies that the hydrophobic *tert*-butyl groups of the calixarene molecules are aligned upwards. Based on the more hydrophilic SiO_2 AFM tip we expect strong interactions between the AFM tip and the TiO_2 surface and weak interactions between the AFM tip and the calixarene molecules. This behavior was investigated on a Si-wafer ALD coated with 80 cycles of TiO_2 and decorated with calixarene. The AFM peak force tapping mode provided information about strong and weak

tip-surface interactions. Figure 4a displays the tip-surface adhesion in pN. With respect to our overall understanding of the surface texture illustrated in Figure 2a heights on the topography map (Figure 2b) correspond to depths on the adhesion map (see Figure 4a) and vice versa. Both maps were recorded simultaneously of the same section of the wafer surface. In comparison, both representations show an inverted contrast. For better visualization cross-sectional views of both representations (yellow trace, Figure 4a) are plotted in Figure 4b (top: adhesion cross-sectional view, bottom: topography cross-sectional view). For clarity the adhesion data was multiplied by the factor (–1) resulting in matching positions for maxima (calixarene) and minima (TiO_2) in both cross-sectional views. This representation of topography and adhesion cross-sections exhibits a large overlap of minima and maxima therefore strongly suggesting the presence of hydrophobic calixarene molecules on the titania-coated wafer surface. Based on the tip-surface adhesion data the forces can be determined as approximately 0 pN for calixarene and 450 pN for TiO_2. Considering several Ti–OH groups contributing to tip-surface interactions, 450 pN are consistent with results from Williams et al., reporting 181 ± 35 pN for single hydrogen bond adhesion forces (OH–OH) [23]. Besides, considering the tip-surface convolution as discussed above the size of isolated features perfectly fits the size of individual calixarene molecules. This furthermore allows for monitoring the distribution of calixarene on a monomolecular level suggesting that the nanopattern predominantly consists of isolated calixarene molecules rather than larger agglomerates. Therefore, the AFM findings directly support the overall idea of creating distinct uniform nanocavities whose shape and size are determined by the choice of p-*tert*-butyl-calix[4]arene as sacrificial template.

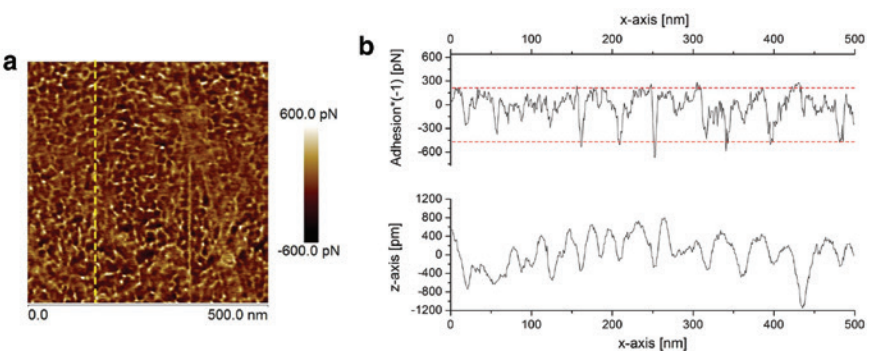

Fig. 4: Representation of the tip-surface adhesion obtained from a Si(100) wafer ALD coated with 80x TiO_2 and decorated with calixarene template molecules using AFM peak force tapping mode: (a) two-dimensional adhesion map, (b) comparison of topography cross-sectional view and adhesion cross-sectional views multiplied by the factor (–1) for clarity.

To assure that nanocavities are solely formed on the wafer surface as a consequence of template application and do not appear in the absence of calixarene, Figure 5 exhibits different representations of the surface of a calixarene-free reference sample, i.e. Si-wafer + 80x TiO_2 + 5x Al_2O_3. Without using calixarene nanotemplates the surface can be expected to be smooth and conformally coated with Al_2O_3 as schematically illustrated in Figure 5a. Figure 5b portrays the two-dimensional wafer surface topography obtained in AFM tapping mode. A three-dimensional representation is shown in Figure 5c, while Figure 5d depicts a cross-sectional view of the topography. As can be seen in all representations, the surface was very smooth and did not exhibit any cavity-like structures in contrast to the surface, where calixarene was grafted prior to ALD (see Figure 3). The two bright regions

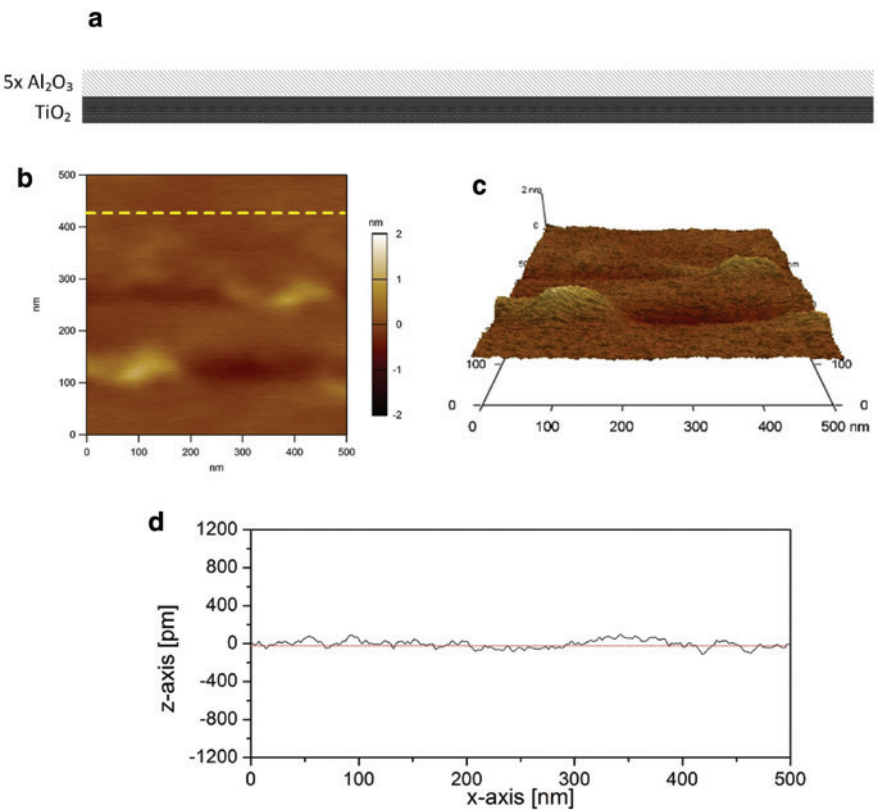

Fig. 5: Variety of representations of the surface topography of a Si(100) wafer ALD coated with 80x TiO_2 and 5x Al_2O_3: (a) schematic illustration of the nanolaminar structure, (b) 2D AFM topography, (c) 3D AFM topography, (d) cross-sectional view of the surface along the yellow trace.

in b) with height variations in the nanometer range reflect unevenness of the initial wafer surface. Thus, owing to the wafer irregularities, the mean roughness is 0.19 ± 0.17 nm, which is higher than expected in this case since it is similar to the mean roughness of the wafer surface containing nanocavities (see above). The mean roughness along the cross-sectional view in Figure 5d is 0.04 nm proving great conformity and smoothness of the deposited metal oxide layers.

4 Conclusions

The feasibility to monitor the template based bottom-up synthesis of nanocavities on a monomolecular level with an AFM is demonstrated. Besides structural surface characterization, chemical analysis was carried out using XPS to identify the TiO_2 and Al_2O_3 ALD layers, which serve as a framework for the nanocavities. In particular, p-*tert*-butyl-calix[4]arene sacrificial template molecules were covalently bound on a titania covered planar Si-wafer creating a nanopattern towards area selective ALD. The size of the observed features resembles the dimension of single calixarene molecules. This observation gives evidence for the presence of isolated calixarene molecules rather than agglomerates. Besides, the mean distance between the calixarene molecules is fully consistent with the mean distance between the nanocavities measured subsequent to Al_2O_3 ALD and thermal O_3 treatment for calixarene template removal. Furthermore, the orientation of the calixarene *tert*-butyl groups is aligned upwards as can be confirmed by comparing topography and adhesion maps and calculating tip-surface adhesion forces. Thus, AFM is a powerful tool for directly evidencing and quantifying template molecules and, in particular, nanocavities. This approach allows for a thorough understanding of processes underlying controlled nanostructuring of oxide surfaces.

Acknowledgements: The authors would like to thank Karl Kopp for performing XPS experiments. Financial support by the Deutsche Forschungsgemeinschaft (DFG-FOR1583) is gratefully acknowledged.

References

1. C. Marichy, M. Bechelany, N. Pinna, Adv. Mater. **24** (2012) 1017.
2. B. J. O'Neill, D. H. K. Jackson, J. Lee, C. Canlas, P. C. Stair, C. L. Marshall, J. W. Elam, T. F. Kuech, J. A. Dumesic, G. W. Huber, ACS Catal. **5** (2015) 1804.
3. N. Sobel, C. Hess, Angew. Chem. Int. Ed. Engl. **54** (2015) 15014.
4. Z. Gao, M. Dong, G. Wang, P. Sheng, Z. Wu, H. Yang, B. Zhang, G. Wang, J. Wang, Y. Qin, Angew. Chem. Int. Ed. Engl. **54** (2015) 9006.

5. J. Lu, J. W. Elam, P. C. Stair, Acc. Chem. Res. **46** (2013) 1806.
6. N. A. Ray, R. P. Van Duyne, P. C. Stair, J. Phys. Chem. C **116** (2012) 7748.
7. S. M. George, Chem. Rev. **110** (2010) 111.
8. P. Ruff, S. Lauterbach, H.-J. Kleebe, C. Hess, Microporous Mesoporous Mater. **235** (2016) 160.
9. J. W. Elam, J. A. Libera, T. H. Huynh, H. Feng, M. J. Pellin, J. Phys. Chem. C **114** (2010) 17286.
10. N. Sobel, C. Hess, M. Lukas, A. Spende, B. Stuhn, M. E. Toimil-Molares, C. Trautmann, Beilstein J. Nanotechnol. **6** (2015) 472.
11. A. Spende, N. Sobel, M. Lukas, R. Zierold, J. C. Riedl, L. Gura, I. Schubert, J. M. Moreno, K. Nielsch, B. Stuhn, C. Hess, C. Trautmann, M. E. Toimil-Molares, Nanotechnology **26** (2015) 335301.
12. C. P. Canlas, J. Lu, N. A. Ray, N. A. Grosso-Giordano, S. Lee, J. W. Elam, R. E. Winans, R. P. Van Duyne, P. C. Stair, J. M. Notestein, Nat. Chem. **4** (2012) 1030.
13. M. Fang, J. C. Ho, ACS Nano **9** (2015) 8651.
14. M. Knez, K. Nielsch, L. Niinistö, Adv. Mater. **19** (2007) 3425.
15. J. Liu, Y. Mao, E. Lan, D. R. Banatao, G. J. Forse, J. Lu, H.-O. Blom, T. O. Yeates, B. Dunn, J. P. Chang, J. Am. Chem. Soc. **130** (2008) 16908.
16. S. Schiwek, L.-O. Heim, R. W. Stark, C. Dietz, J. Appl. Phys. **117** (2015) 104303.
17. A. Voss, R. W. Stark, C. Dietz, Macromolecules **47** (2014) 5236.
18. H. J. Butt, M. Jaschke, Nanotechnology **6** (1995) 1.
19. A. Rosa-Zeiser, E. Weilandt, S. Hild, O. Marti, Meas. Sci. Technol. **8** (1997) 1333.
20. P. M. Spizig, Dynamische Rasterkraftmikroskopie, Faculty of Natural Sciences, University of Ulm (2002).
21. P. J. de Pablo, J. Colchero, J. Gomez-Herrero, A. M. Baro, Appl. Phys. Lett. **73** (1998) 3300.
22. C. Hess, in *Nanostructured Catalysts: Selective Oxidations* (Eds.: C. Hess, R. Schlögl), RSC Nanoscience & Nanotechnology No. 19, Ch. 13, Cambridge (2011).
23. J. M. Williams, T. Han, T. P. Beebe Jr., Langmuir **12** (1996) 1291.

Supplemental Material: The online version of this article offers supplementary material (https://doi.org/10.1515/zpch-2017-1055).